processes

MDPI

Article

Enhancing the Surface Quality of FDM Processed Flapping Wing Micro Mechanism Assembly through RSM–TOPSIS Hybrid Approach

Devaraj Rajamani [1], Esakki Balasubramanian [1,*] and Lung-Jieh Yang [2]

[1] Centre for Autonomous System Research, Department of Mechanical Engineering, Vel Tech Rangarajan Dr. Sagunthala R&D Institute of Science and Technology, Chennai 600062, India
[2] Department of Mechanical and Electro-Mechanical Engineering, Tamkang University, New Taipei City 251301, Taiwan
* Correspondence: esak.bala@gmail.com

Abstract: Improving surface quality attributes is a critical task in the production of micro-sized near-net-shaped components for end-use applications using additive manufacturing techniques. In the present study, we investigated the effect of fused deposition modeling (FDM) process parameters such as layer thickness, part orientation, raster width and raster angle on the surface quality characteristics of as-fabricated test specimens in order to develop the assembly of a flapping wing micro mechanism. Through a Box–Behnken design, a suitable experimental strategy was developed, and test specimens were manufactured. The performance of the experiments was statistically assessed using multi-response analysis of variance (ANOVA). The microstructures of the test specimens produced with various processing parameters were examined using a scanning electron microscope to identify micro surface flaws under various processing conditions. Furthermore, the optimal FDM parameters for improved surface quality attributes such as Ra, Rz and Rq were obtained using a statistical optimization technique known as Technique for Order of Preference by Similarity to Ideal Solution (TOPSIS).

Keywords: fused deposition modeling; additive manufacturing; micro mechanism; optimization; analysis of variance; surface quality

check for updates

Citation: Rajamani, D.; Balasubramanian, E.; Yang, L.-J. Enhancing the Surface Quality of FDM Processed Flapping Wing Micro Mechanism Assembly through RSM–TOPSIS Hybrid Approach. *Processes* **2022**, *10*, 2457. https://doi.org/10.3390/pr10112457

Academic Editor: Sara Liparoti

Received: 28 October 2022
Accepted: 17 November 2022
Published: 19 November 2022

Publisher's Note: MDPI stays neutral with regard to jurisdictional claims in published maps and institutional affiliations.

Copyright: © 2022 by the authors. Licensee MDPI, Basel, Switzerland. This article is an open access article distributed under the terms and conditions of the Creative Commons Attribution (CC BY) license (https://creativecommons.org/licenses/by/4.0/).

1. Introduction

The fabrication of micro mechanical components imposes significant challenges in terms of dimensional accuracy, surface finish, mechanical strength characteristics and weight burden in the development of micro aerial vehicles [1–3]. Computer-aided design (CAD) and analysis play a significant role in the design and assembly of micro mechanical components. To prototype the parts for easy and quick realization, 3D printing is an efficient choice. Conventional methods of fabricating micro mechanism parts such as injection molding, wire cut EDM, casting and forging are time-consuming and labor-intensive, and the cost involvement is high. The modification and fabrication of various parts' features are cumbersome and expensive with conventional subtractive manufacturing processes. Manufacturing parts from CAD data is not possible with these processes [4].

Additive manufacturing (AM) is a cost-effective process and realizes the parts' fabrication in a swift manner. It avoids the need for jigs, fixtures, preparation of molds and other pre-processing steps in the manufacturing of micro components. The intricate features of micro mechanism parts are difficult to manufacture using conventional processes. However, AM techniques can be utilized to fabricate micro-level, complex and intricate parts with suitable dimensional accuracy. It has minimum wastage of materials in comparison to conventional manufacturing processes. The human intervention to fabricate micro parts with minimal efforts is an advantage of using AM in various applications. The polymer-based

fabrication of micro components using fused deposition modeling is predominantly used in various applications such as the automotive, aerospace, medical and toy industries [5]. A variety of polymers such as polystyrene (PS), poly ether ether ketone (PEEK), polypropylene (PP), polylactic acid (PLA), polycarbonate (PC) and other polymer materials are used for various AM technologies. However, the usage of acryl butadiene styrene (ABS) material in FDM has achieved superior mechanical strength characteristics and dimensional accuracy. Many pioneering research works on FDM to assess the mechanical behavior, surface roughness and dimensional accuracy of the fabricated parts have been performed. Altan et al. [6] studied the influence of various FDM process parameters on the surface roughness and tensile strength characteristics of PLA-based parts. Camphell et al. [7] explored the surface roughness characteristics of parts made with ABS materials using FDM. There are many factors such as layer thickness, bed temperature, printing speed, slicing of layer, build orientation, raster angle, width, extrusion temperature, infill rate and other FDM process parameters affecting the part quality. Yang et al. [8] performed optimization studies on selecting the optimal process parameters of the FDM process to achieve high tensile strength and low surface finish of PLA parts. Magdum et al. [9] investigated the effect of infill density, layer thickness and shell thickness of the FDM process and examined the influence of these parameters on the mechanical properties of parts fabricated using PLA material. Vikas et al. [10] explored the influence of various process parameters such as layer thickness, printing temperature and speed on the mechanical characteristics of PLA parts made using FDM. Camargo et al. [11] studied the combination of using PLA–graphene material for evaluating the tensile strength of parts made using FDM. The infill rate and layer thickness are the major factors that affect the part quality. Vigneshwaran et al. [12] conducted various experimental investigations on the evaluation of the mechanical characteristics of the composite structures of biodegradable wood and PLA made with the FDM technique. Recently, several researchers have employed 3D printing to fabricate micro mechanical parts for achieving a high strength-to-weight ratio and improved dimensional stability. Carlo Ferro et al. [13] elaborated the significance of additive manufacturing the components of an unmanned aerial vehicle (UAV) using fused deposition modeling (FDM). Kramer explored the fabrication of flapping wing veins using 3D printing with a polylactic acid (PLA) material. Hsu et al. [14] realized micro gears and tiny linkages using Multijet 3D printing. Richter and Lipson [15] utilized polyjet 3D printing technology for fabricating the wings of micro insects. The author's earlier works on 3D printing of various micro mechanical components of flapping wing micro aerial vehicle and unmanned aerial vehicle structures have provided further insight on realizing the linkage mechanism parts quickly. It was observed that the surface finish of 3D-printed micro mechanism parts is significantly affected by the part assembly process. The functionality of a prototype depends on the appearance of tiny parts that are essential to showcase as a product.

The extensive literature review revealed that within a decade, AM technologies became widely used for the creation of complex 3D components. Through the application of several crucial adjustments and upgrades to obtain the ideal circumstances for microfabrication, some specialized AM technologies are also capable of producing 3D micro parts and structures. Among the scalable AM technologies, FDM is found to be a suitable technique for fabricating complex geometries due to their simple working mechanism, minimized materials and low processing costs. Few reports exist on the use of FDM for the production of truly sophisticated 3D micro parts [16–19]. Most micro parts created using FDM are used in biomedical applications, and a few researchers have created micro parts for mechanical applications, particularly for flapping wing vehicles. Furthermore, the optimization of FDM parameters for enhancing the quality and performance characteristics of micro components is limited; thus, the exploration of this aspects is needed.

Therefore, the present work focuses on exploring the surface roughness characteristics of FDM-printed micro mechanical parts. The test samples were fabricated as per the Box–Behnken design of response surface methodology. The statistical analyses of performed experiments were assessed through analysis of variance, and the impacts of selected

process parameters such as layer thickness, part orientation, raster width and raster angle on surface quality characteristics such as *Ra*, *Rz* and *Rq* were investigated through the aid of three-dimensional response surface plots. The optimal FDM parameters for improving surface quality were attained through TOPSIS optimization. Moreover, the microstructures of as-fabricated test specimens under different processing conditions were investigated through scanning electron microscopy.

2. Methodology

2.1. Response Surface Methodology

Response surface methodology (RSM) is an empirical statistical modeling technique used for optimizing complex processes [20]. It provides an easy and efficient technique to find the best range of design space for performance. RSM aims at approximating it by a suitable lower-order polynomial, especially a second-order polynomial equation. The quadratic response surface is used to correlate the relationship between independent variables (X_i) and response (Y) as follows:

$$Y = b_0 + \sum_{i=1}^{n} b_i X_i + \sum_{i=1}^{n} b_{ii} X_i^2 + \sum_{i<j}^{n} b_{ij} X_i X_j \quad (1)$$

where n is the number of design variables, and b_0, b_i, b_{ii} and b_{ij} represent the coefficients of constant, linear, quadratic and cross-product terms, respectively.

To obtain a proper model for the optimization of the FDM process parameters, Box–Behnken design (BBD), which is a type of RSM, was selected in this study, with four process variables at three levels. The BBD is normally used when performing non-sequential experiments, and these designs allow efficient estimation of first- and second-order coefficients with fewer design points to reduce the number of experiments. In the present study, experiments were performed according to the BBD experimental design to obtain a quadratic model consisting of twenty-nine experiments, to identify the optimum conditions and study the effect of process variables on the FDM process. Design Expert™ software version 8.0 was used to obtain the predicted values through a model fitting technique.

2.2. The Technique for Order of Preference by Similarity to Ideal Solution (TOPSIS)

To obtain the best optimal solution among available alternatives, a statistical multi-criteria decision-making approach, TOPSIS, has been widely used for solving complex real-world problems. In TOPSIS, the multi-objective problems are converted into a single objective to achieve an optimal solution. The smallest and longest distances from the optimistic and negative ideal solutions, respectively, are the most important options as determined by TOPSIS. The step-by-step procedure of TOPSIS for solving general engineering problems is given below [21]:

Step 1: The evaluation matrix is constructed for m alternatives and n criteria.

$$M_E = \begin{pmatrix} x_{11} & x_{12} & \cdots & x_{1n} \\ x_{21} & x_{22} & \cdots & x_{2n} \\ \vdots & \vdots & & \vdots \\ x_{m1} & x_{m2} & \cdots & x_{mn} \end{pmatrix} \quad (2)$$

where x_{mn} denotes the performance of the mth alternative for the nth attribute.

Step 2: A normalized performance matrix for i and j is formulated through the following relation.

$$\beta_{ij} = \frac{Y_{ij}}{\sqrt{\sum_{i=1}^{m} Y^2{}_{ij}}} \quad (3)$$

where β_{ij} indicates the normalized value for $i = 1, 2, 3, \ldots, m$ and $j = 1, 2, 3, \ldots, n$.

Step 3: The weight function for individual response characteristics is calculated using a compromised weighting approach. The present work utilizes the combined entropy and analytical hierarchy process for assigning the weights of individual responses. The weight for the *i*th criteria is calculated as follows:

$$w_i = \frac{\phi_i \times \varphi_i}{\sum_{i=1}^{n} \phi_i \times \varphi_i} \quad i = 1, \ldots, n \tag{4}$$

$$\varphi_i = \frac{1 - a_i}{\sum_{i=1}^{n} (1 - a_i)} \tag{5}$$

where w_i indicates the weight of the *i*th attribute, and φ_i and ϕ_i denote the weight of the *i*th criteria obtained through the entropy method and the AHP approach. The weighted and normalized design matrix is formulated through the following relation:

$$\eta_{ij} = \beta_{ij} \times w_i \tag{6}$$

Step 4: The beneficial and non-beneficial responses were utilized for calculating the positive (S^+) and negative (S^-) ideal solutions.

$$\sigma^+ = {\sigma_1}^+, {\sigma_2}^+, \ldots {\sigma_n}^+ = \left\{ \left(\max \sigma_{ij} | j \in K \right), \left(\min \sigma_{ij} | j \in K' \right) | i = 1, 2, \ldots, n \right\} \tag{7}$$

$$\sigma^- = {\sigma_1}^-, {\sigma_2}^-, \ldots {\sigma_n}^- = \left\{ \left(\max \sigma_{ij} | j \in K \right), \left(\min \sigma_{ij} | j \in K' \right) | i = 1, 2, \ldots, n \right\} \tag{8}$$

where K indicates the index set for the beneficial response and K' indicates the index set for the non-beneficial response.

Step 5: The ideal solutions are utilized for calculating the distance for respective response characteristics as follows:

$${S_i}^+ = \left\{ \sum_{j=1}^{n} \left(\sigma_{ij} - {\sigma_j}^+ \right)^2 \right\}^{0.5} \tag{9}$$

$${S_i}^- = \left\{ \sum_{j=1}^{n} \left(\sigma_{ij} - {\sigma_j}^- \right)^2 \right\}^{0.5} \tag{10}$$

where $j = 1, 2, \ldots, n$; $i = 1, 2, \ldots, m$.

Step 6: The closeness coefficient (C_i) value for individual ideal experimental solutions is computed using the following relation:

$$C_i = \frac{{S_i}^-}{{S_i}^- + {S_i}^+} \tag{11}$$

A higher value of C_i indicates that the rank is better.

3. FDM Experimentation and Measurements

The experiments were conducted, and test specimens were fabricated using a Fortus 250 mc commercial additive manufacturing machine with maximum part-built size capability of 254 × 254 × 305 mm^3, manufactured by Stratasys Inc., Eden Prairie, MN, USA. Acrylonitrile butadiene styrene (ABS) [$(C_8H_8 \cdot C_4H_6 \cdot C_3H_3N)_n$] polymer filament was used as the part material for the prototype model. The three-dimensional solid part was created by SolidWorks software™ and linked to Stratasys software for pre-processing part-built operations. The cylindrical FDM test specimens of dimensions 15 mm × 15 mm were fabricated by melting and extruding the thermoplastic material through heating of the part material deposition nozzle. The solidifying material distributed from the nozzle was deposited onto the surface of the platform to make the first layer. This procedure was repeated until the 3D physical part model was obtained. Four factors, namely layer

thickness (x_1), part orientation (x_2), raster width (x_3) and raster angle (x_4), were considered as process input parameters while keeping other parameters such as contour width, air gap and part fill style at fixed levels. The parameters and their levels were selected according to the pilot experiments, existing literature and guidelines given by the manufacturer. The details of the selected FDM parameters and their corresponding levels are shown in Table 1. The surface roughness characteristics such as average roughness (*Ra*), average maximum height of the profile (*Rz*) and root mean square roughness (*Rq*) of the FDM specimens were measured using the non-contact optical universal 3D profilometer (Make: Rtec Instruments, Silicon Valley, CA, USA). The average surface roughness parameters were calculated by taking the observations on the top, side and bottom surfaces of the test specimens. For each specimen, the roughness values were assessed thrice, and their average values were taken into consideration to avoid measurement errors. The FDM system utilized for fabricating the test specimens, the fabricated test specimens and the measurement of roughness parameters are shown in Figure 1. The experimentally measured surface roughness characteristics values are given in Table 2.

Table 1. FDM process parameters and levels.

Factor	Symbol	Level			Unit
		Low	Medium	High	
Layer thickness	*A*	0.127	0.228	0.33	mm
Part orientation	*B*	0	45	90	Degree
Raster width	*C*	0.203	0.381	0.558	mm
Raster angle	*D*	0	30	60	Degree

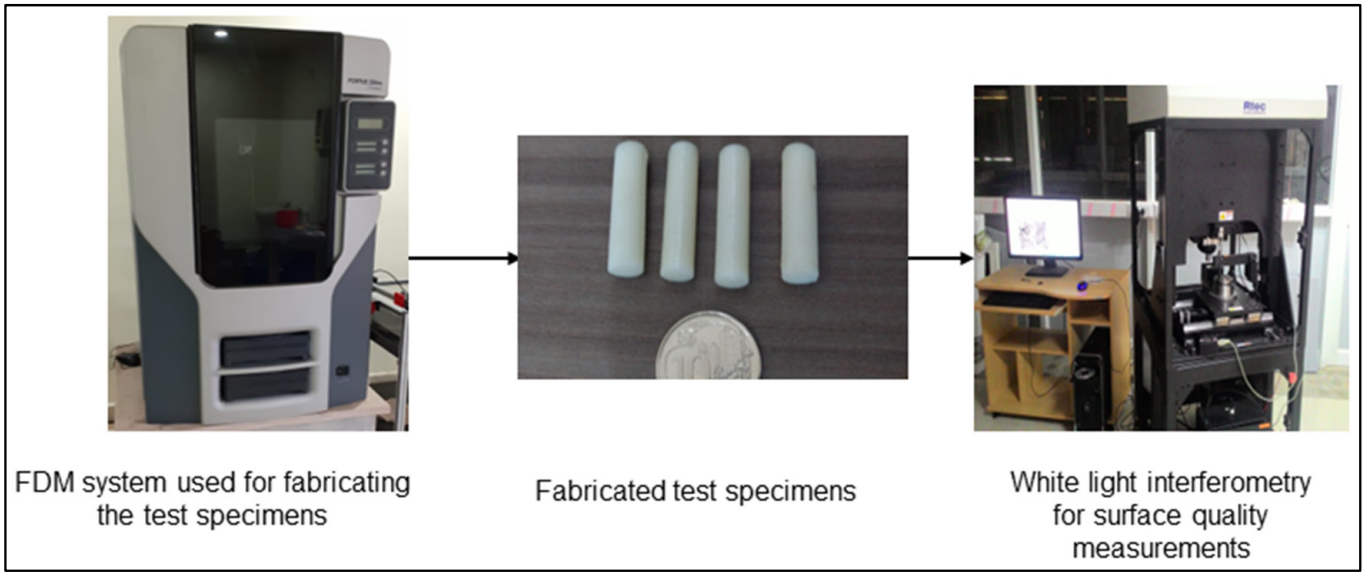

Figure 1. FDM process and surface roughness measurements.

Table 2. FDM experimental design and measured responses.

Exp. No	Input Parameters				Response Characteristics		
	Layer Thickness (mm)	Part Orientation (°)	Raster Width (mm)	Raster Angle (°)	*Ra* (μm)	*Rz* (μm)	*Rq* (μm)
1	0.2285	45	0.558	0	25.8	98.3	49.4
2	0.2285	45	0.3805	30	27.2	96.8	46.3
3	0.2285	90	0.203	30	25.9	95.9	47
4	0.33	45	0.558	30	27.7	96.1	44.3
5	0.2285	0	0.3805	0	23.4	104.1	48.6
6	0.33	90	0.3805	30	23.6	105.7	44.7
7	0.2285	45	0.3805	30	27.5	98.1	46.4
8	0.2285	45	0.203	60	26.8	93.6	50.9
9	0.127	45	0.3805	60	26.6	96.3	51.2
10	0.2285	45	0.203	0	27.3	100.8	49.7
11	0.2285	0	0.558	30	26.7	98.5	46.8
12	0.2285	0	0.3805	60	27.9	94.9	49.8
13	0.2285	45	0.3805	30	27.1	97.3	46.6
14	0.2285	90	0.3805	0	26.1	98.4	48.1
15	0.2285	90	0.3805	60	22.2	102.1	48.8
16	0.127	45	0.558	30	26.4	104.2	48.7
17	0.33	45	0.3805	60	26.5	101.3	47.8
18	0.127	45	0.3805	0	25.5	102.5	49.1
19	0.2285	45	0.558	60	26.9	99.4	49.9
20	0.2285	90	0.558	30	24.1	101.7	45.2
21	0.2285	45	0.3805	30	27.5	97.5	46.5
22	0.33	45	0.203	30	27.6	103.8	47.1
23	0.127	0	0.3805	30	24.5	99.8	47.5
24	0.2285	0	0.203	30	26.2	96.4	46.9
25	0.2285	45	0.3805	30	27.4	96.5	46.7
26	0.127	45	0.203	30	28.1	91.5	47.4
27	0.33	0	0.3805	30	27.8	100.4	44.2
28	0.127	90	0.3805	30	25.7	97.1	46.1
29	0.33	45	0.3805	0	27	102.9	48.3

4. Result and Discussions

To investigate the efficacy of the experimental strategy, statistical analysis of the performed experiments and the obtained response characteristics is required. The coefficient of determination, sum of squares, lack of fit, individual, interaction, quadratic effects and F-statistics were investigated using multi-parametric analysis of variance (ANOVA) for selected responses, i.e., *Ra*, *Rz* and *Rq*, of the fabricated test specimens in three stages. ANOVA was used in the initial stage to examine the statistical significance and the significance of a few independent variables that influence the performance and quality attributes of surface quality indices. The second stage involved creating second-order polynomial equations for each response to determine the correlations between the chosen dependent variables on the surface quality. In the third phase, the most favorable parametric combinations were determined using the TOPSIS multi-criteria decision-making approach.

4.1. Statistical Analysis of Proposed Regression Models

The FDM experiments were performed based on the proposed RSM-based experimental strategy, and the test specimens were fabricated. The efficiency of formulated mathematical models was statistically investigated through ANOVA. The statistical analysis results for the considered response features *Ra*, *Rz* and *Rq* are shown in Tables 3–5. The ANOVA was performed at a 95% confidence interval for all the response characteristics, and the insignificant parameters consisting of F-values above 0.05 were eliminated through the backward elimination technique. From the ANOVA, the selected FDM parameters were found to be statistically significant if the individual influence was considered. Furthermore,

the layer thickness and raster angle were found to be the most significant parameters on *Rz* and *Rq*, whereas *Ra* was significantly influenced by part orientation. The co-efficient of determination (R2) and the adequate precision at selected design points for *Ra*, *Rz* and *Rq* were 99.57, 97.41 and 99.71 and 57.97, 24.82 and 69.67, respectively, showing the adequacy of the conceived regression models. In addition to ANOVA, the normal probability plots shown in Figure 2a–c indicate the eventual distribution of data points along the center line, proving the statistical significance of the developed models.

Table 3. Statistical analysis for *Ra*.

Source	Sum of Squares	df	Mean Square	F-Value	*p*-Value	
Model	61.42	14	4.39	229.32	<0.0001	Significant
Layer thickness	0.9633	1	0.9633	50.35	<0.0001	
Part orientation	6.6	1	6.6	345.03	<0.0001	
Raster width	1.54	1	1.54	80.54	<0.0001	
Raster angle	0.27	1	0.27	14.11	0.0021	
AB	7.29	1	7.29	381.06	<0.0001	
AC	0.81	1	0.81	42.34	<0.0001	
AD	0.64	1	0.64	33.45	<0.0001	
BC	1.32	1	1.32	69.13	<0.0001	
BD	17.64	1	17.64	922.07	<0.0001	
CD	0.64	1	0.64	33.45	<0.0001	
A^2	0.1287	1	0.1287	6.72	0.0213	
B^2	19.94	1	19.94	1042.3	<0.0001	
C^2	0.1912	1	0.1912	9.99	0.0069	
D^2	3.8	1	3.8	198.86	<0.0001	
Residual	0.2678	14	0.0191			
Lack of fit	0.1358	10	0.0136	0.4116	0.8838	Not significant
Pure error	0.132	4	0.033			
Cor total	61.69	28				
R^2	99.57	Adj. R^2	99.13	AP	57.97	

Table 4. Statistical analysis for *Rz*.

Source	Sum of Squares	df	Mean Square	F-Value	*p*-Value	
Model	324.03	14	23.15	37.63	<0.0001	Significant
Layer thickness	29.45	1	29.45	47.89	<0.0001	
Part orientation	3.85	1	3.85	6.27	0.0253	
Raster width	21.87	1	21.87	35.56	<0.0001	
Raster angle	31.36	1	31.36	51	<0.0001	
AB	16	1	16	26.02	0.0002	
AC	104.04	1	104.04	169.16	<0.0001	
AD	5.29	1	5.29	8.6	0.0109	
BC	3.42	1	3.42	5.56	0.0334	
BD	41.6	1	41.6	67.64	<0.0001	
CD	17.22	1	17.22	28	0.0001	
A^2	30.71	1	30.71	49.93	<0.0001	
B^2	11.84	1	11.84	19.25	0.0006	
C^2	1.62	1	1.62	2.63	0.1273	
D^2	10.98	1	10.98	17.85	0.0008	
Residual	8.61	14	0.615			
Lack of fit	7.06	10	0.7058	1.82	0.2962	Not significant
Pure error	1.55	4	0.388			
Cor total	332.64	28				
R^2	97.41	Adj. R^2	94.82	AP	24.82	

Table 5. Statistical analysis for *Rq*.

Source	Sum of Squares	df	Mean Square	F-Value	*p*-Value	
Model	94.84	14	6.77	341.75	<0.0001	Significant
Layer thickness	15.41	1	15.41	777.61	<0.0001	
Part orientation	1.27	1	1.27	63.95	<0.0001	
Raster width	1.84	1	1.84	92.87	<0.0001	
Raster angle	2.25	1	2.25	113.68	<0.0001	
AB	0.9025	1	0.9025	45.53	<0.0001	
AC	4.2	1	4.2	212.02	<0.0001	
AD	1.69	1	1.69	85.26	<0.0001	
BC	0.7225	1	0.7225	36.45	<0.0001	
BD	0.0625	1	0.0625	3.15	0.0975	
CD	0.1225	1	0.1225	6.18	0.0262	
A^2	0.447	1	0.447	22.55	0.0003	
B^2	2.34	1	2.34	117.81	<0.0001	
C^2	2.34	1	2.34	117.81	<0.0001	
D^2	54.08	1	54.08	2728.5	<0.0001	
Residual	0.2775	14	0.0198			
Lack of fit	0.1775	10	0.0177	0.71	0.7	Not significant
Pure error	0.1	4	0.025			
Cor total	95.11	28				
R^2	99.71	Adj. R^2	99.42	AP	69.67	

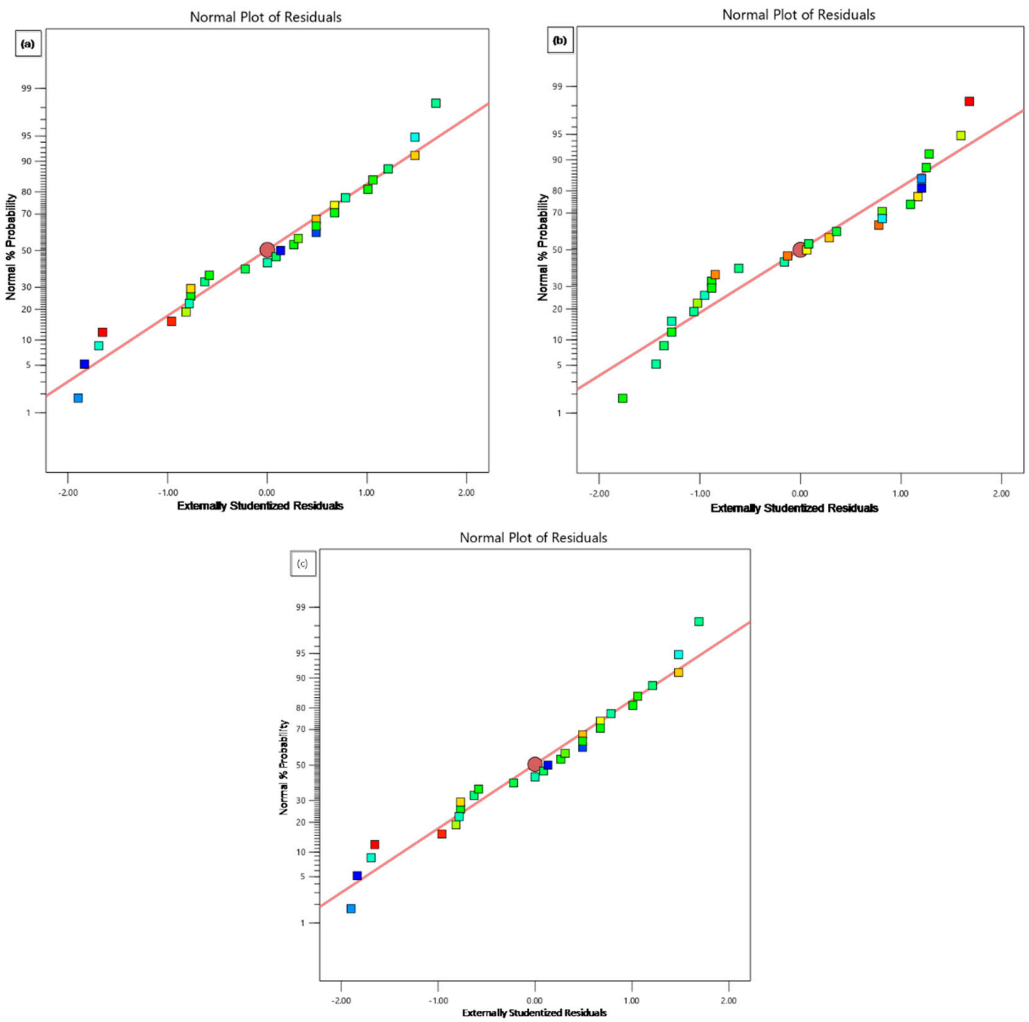

Figure 2. Normal probability plots for (**a**) *Ra*, (**b**) *Rz* and (**c**) *Rq*.

4.2. Influence of FDM Parameters on Surface Quality Characteristics

Since surface roughness affects a product's functionality in each condition, it is crucial for engineering applications and should be minimized, especially for bearings, gears, guideways and applications that are prone to fatigue loading [22]. The statistical investigation results show that the selected FDM parameters significantly influenced the surface roughness characteristics of fabricated test specimens. During the FDM process, the presence of abundant process- and material-related parameters leads to a complex processing mechanism which results in inferior dimensional accuracy and poor surface quality due to the non-uniform heating and cooling cycles and the accumulation of internal stresses [23,24]. Therefore, it is necessary to investigate the influence of process parameters on the quality and performance characteristics and use components fabricated through fused deposition modeling. The interactive consequences of FDM parameters on the selected response features of *Ra*, *Rz* and *Rq* were investigated through three-dimensional response surface plots, as shown in Figures 3–5.

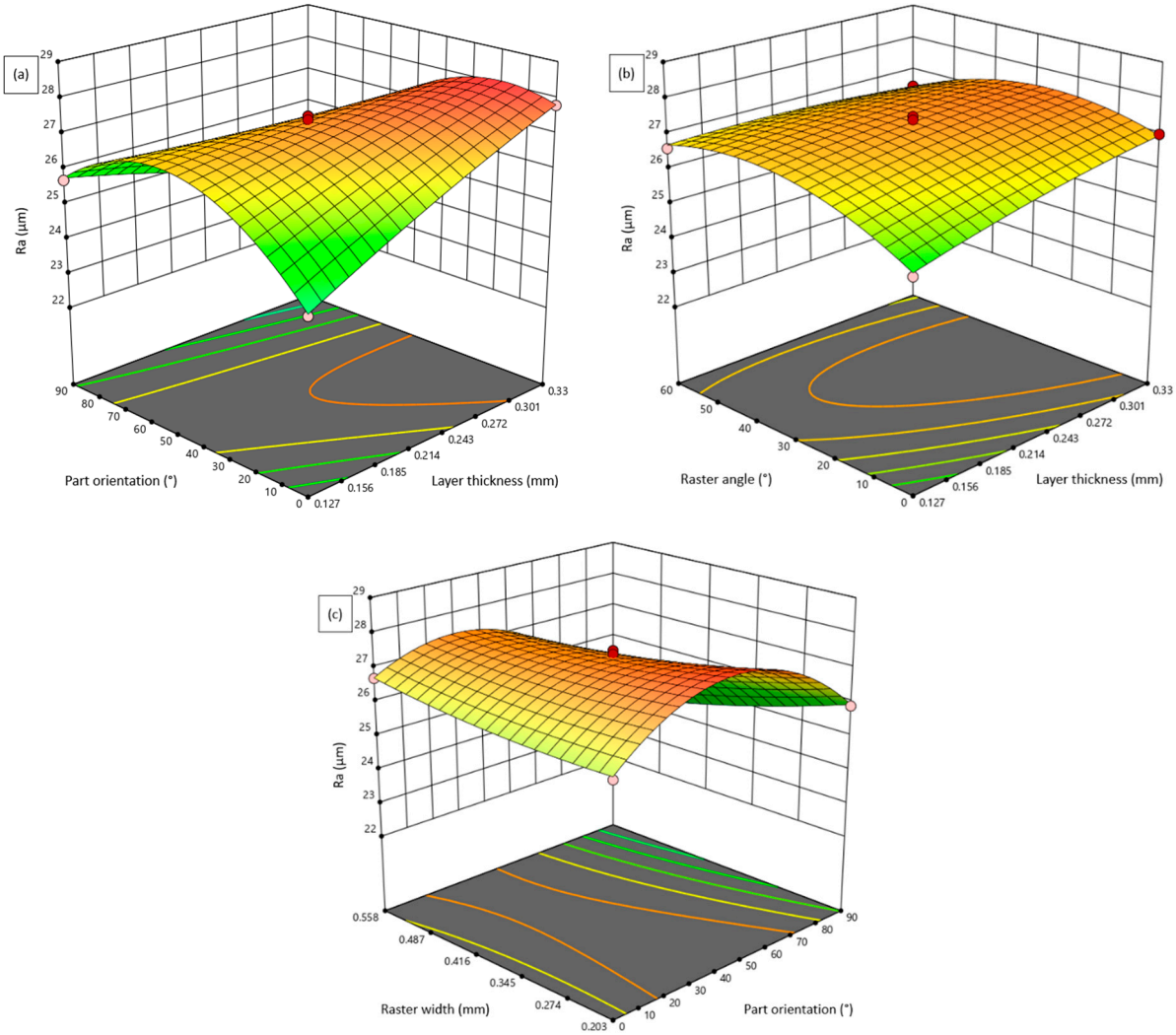

Figure 3. Influence of FDM parameters on *Ra*: (**a**) Layer thickness vs. Part orientation; (**b**) Layer thickness vs. Raster angle; and (**c**) Part orientation vs Raster width.

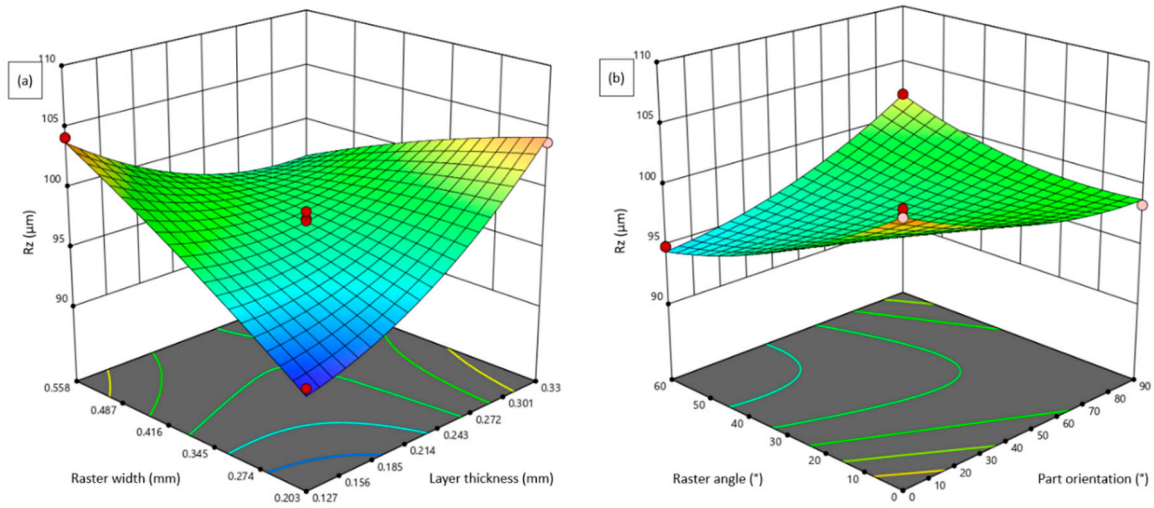

Figure 4. Influence of FDM parameters on *Rz*: (**a**) Layer thickness vs. Raster width; and (**b**) Part orientation vs. Raster angle.

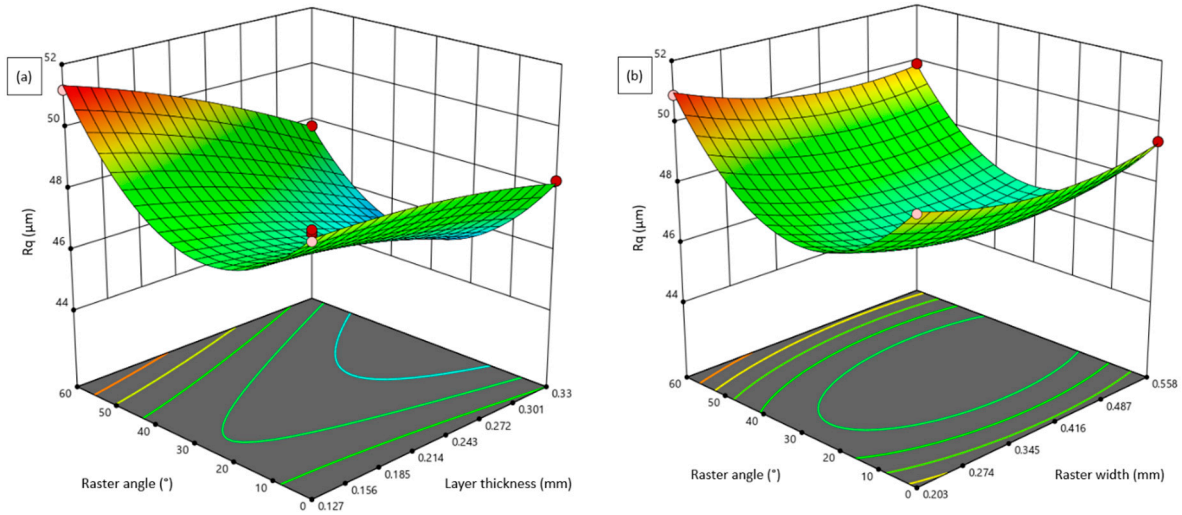

Figure 5. Influence of FDM parameters on *Rq*: (**a**) Layer thickness vs. Raster angle; and (**b**) Raster angle vs. Raster width.

In the FDM process, the thickness of each layer deposited by the nozzle was decided based on the geometrical complexity of the part, printing time and required surface quality. From the statistical analysis, the layer thickness has a substantial influence on the selected surface roughness properties. Figures 3a, 4a and 5a show the influence of layer thickness on surface roughness characteristics. The response surface plots indicate that the increase in layer thickness from 0.127 mm to 0.33 mm drastically diminished the roughness characteristics. As the layer thickness increased, the stair-stepping effect significantly increased, which prominently augmented the roughness of fabricated parts in all directions; hence, the surface quality was diminished at higher layer thickness [25]. Therefore, it is necessary to maintain low layer thickness to achieve an improved surface quality. Among the selected FDM process parameters, the layer thickness was found to have a more significant impact on the surface quality. Figure 6 shows the sample three-dimensional surface roughness profiles taken on the test specimens fabricated at different layer thicknesses. The roughness parameters *Ra*, *Rz* and *Rq* increased linearly when the thickness of printing layers increased from 0.1 mm to 0.3 mm. In addition to response surface plots, for the investigation of micro surfaces, FDM components fabricated at different layer thicknesses are depicted in Figure 7a–c. From the microstructure observations, it is evident that the

specimens fabricated at a higher layer thickness (0.33 mm) have massive defects, such as raster overlapping, abbreviated voids and pores due to the influence of staircase effects. Moreover, the surface defects between the successive layers are found to be minimal for the specimens fabricated at 0.2285 mm, whereas a defect-free dense structure is observed for the specimens fabricated with low layer thickness (0.128 mm). Therefore, it is necessary to maintain low layer thickness for the fabrication of micro components through the FDM process to achieve quality parts without the presence of defects fashioned by staircase effects [24,26,27].

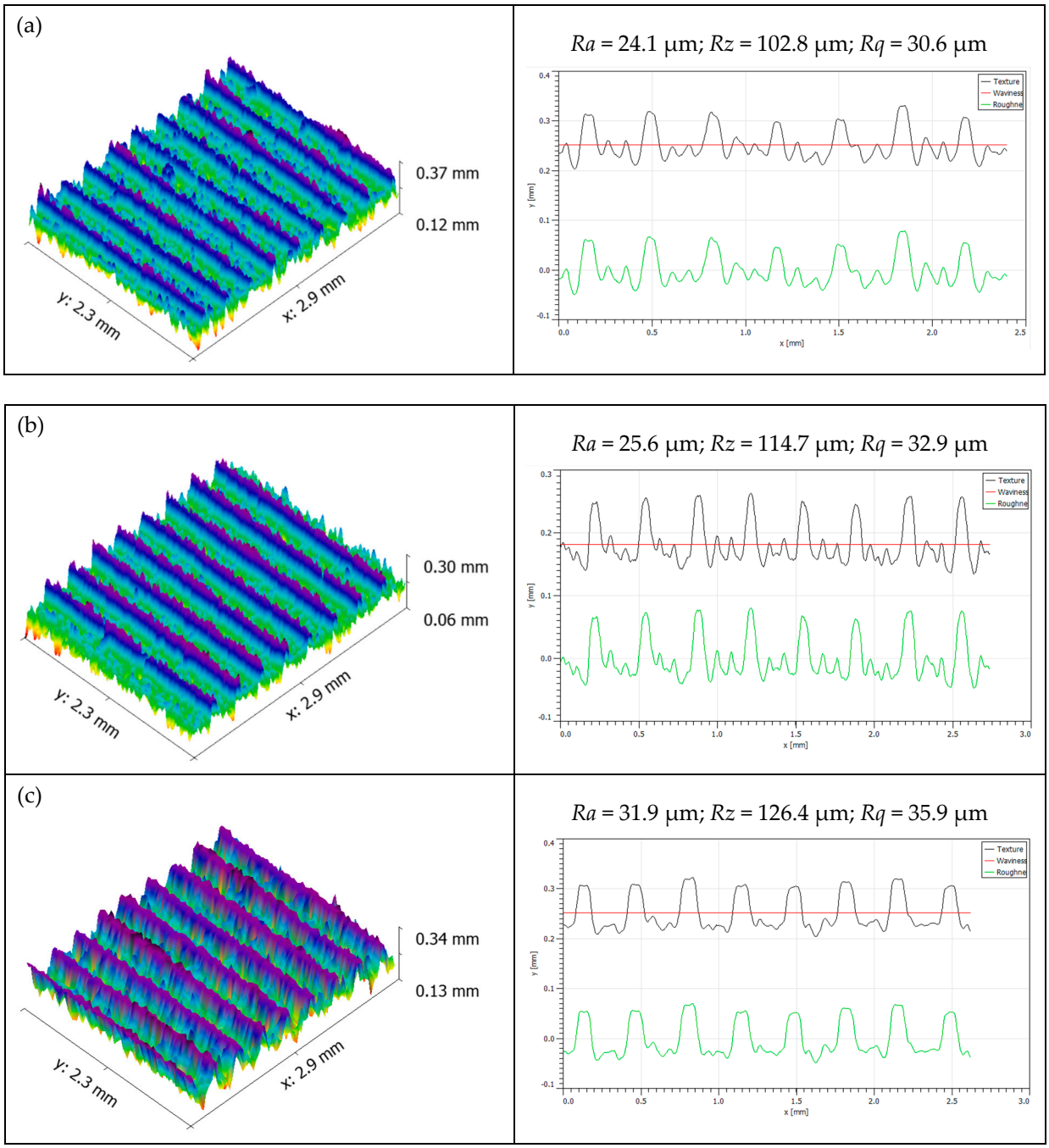

Figure 6. White light interferometry 3D surface profiles for samples fabricated at different layer thicknesses of (**a**) 0.1 mm, (**b**) 0.2 mm and (**c**) 0.3 mm.

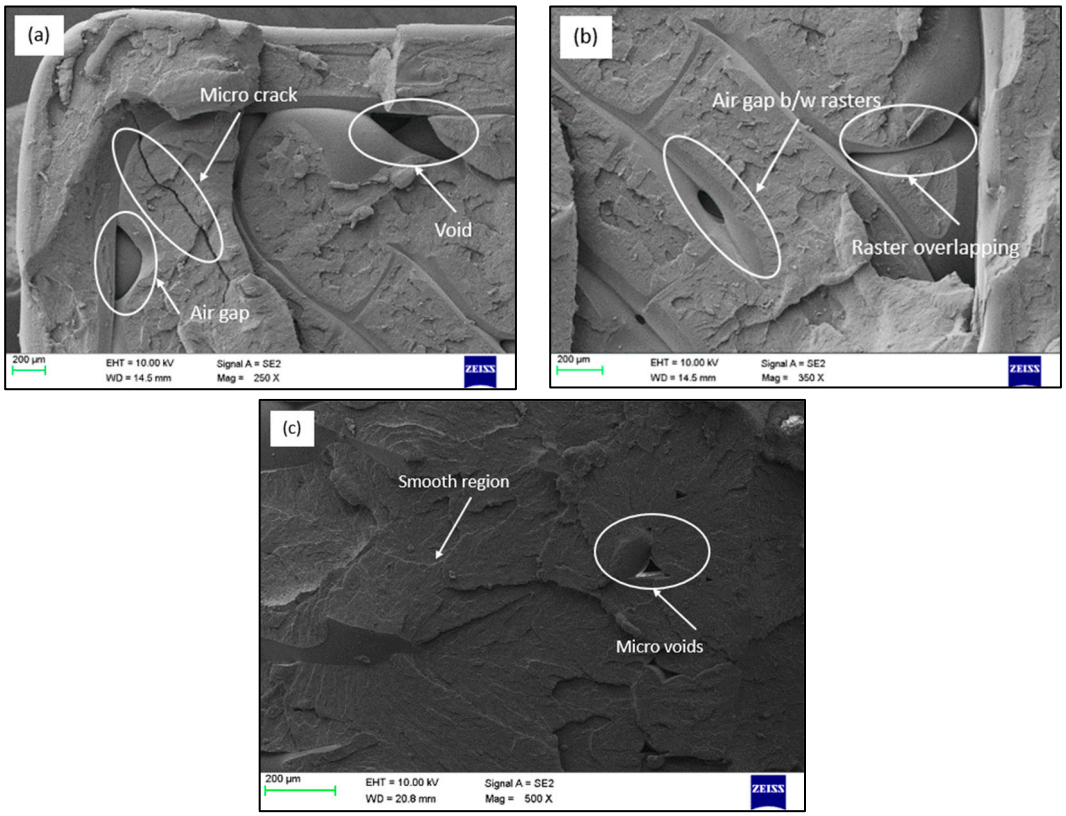

Figure 7. SEM microstructure of FDM components at different processing conditions: (**a**) layer thickness of 0.33 mm; (**b**) layer thickness of 0.2285 mm; (**c**) layer thickness of 0.127 mm.

The influence of part orientation on the surface quality characteristics is demonstrated in Figures 3a,c and 4b. It is evident from the surface plots that the roughness values slightly increased when the parts were fabricated at 45° orientation, whereas the specimens fabricated at 0° and 90° orientation were found to be of better surface quality. When the parts were fabricated at an inclined orientation, the staircase effect increased and thus the roughness increased, whereas the specimens fabricated with horizontal and vertical orientations had significantly improved surface quality parameters despite the complex part profiles [28,29]. The consequences of varying the width of the deposited layer of pattern or raster width are depicted in response surfaces shown in Figures 3c, 4a and 5b. It is perceived that the increase in raster width from 0.203 mm to 0.558 mm resulted in a significant augmentation in the selected response features *Ra*, *Rz* and *Rq*. This could be because the gap between two successive layers deposited in the same direction increased at a higher raster width, and hence the probability of pores and voids between the printed layers increased [30]. Therefore, the roughness values at a higher raster width increased prominently.

The raster angle is a vital parameter in FDM process in which the angle of deposition of the material is varied with respect to the axis of the built table. The influence of the raster angle on *Ra*, *Rz* and *Rq* is demonstrated in the 3D response surface plots in Figures 3b, 4b and 5a,b. The roughness characteristics were found to vary non-linearly for individual response features. The response of *Ra* slightly increased with an increase in raster angle from 0° to 60° and the *Rq* slightly decreased and then increased with an increase in raster angle to a certain value, whereas the *Rz* decreased with an increase in raster angle. In general, an increase in raster angle leads to an increase in the number of rasters with short lengths, which leads to an increase in the number of heating and cooling cycles [31]. As a result of improper thermal deformation, an inadequate surface finish was yielded. For the specimens built with a minimum raster angle and build orientation, a

better surface finish was noted. The number of heating and cooling cycles decreased by using a minimum raster angle and building orientation, which lowers non-uniform thermal stress and distortion. As a result, the road width is straighter, and the surface finish is better [25].

4.3. Multi-Response Optimization Using TOPSIS

The goal of the present investigation was to improve the surface quality characteristics of FDM-fabricated ABS specimens by minimizing roughness values such as *Ra*, *Rz* and *Rq* through optimizing the process parameters using the TOPSIS multi-response optimization technique. The relative weights for each response were calculated through a compromised weighting method, namely the analytical hierarchy approach. Through Equations (4) and (5), the following individual weights were obtained: *Ra*, 0.33919; *Rz*, 0.32974; and *Rq*, 0.33107.

The separation measures (*Si*+, *Si*−) for the weight normalized matrix, closeness coefficient (*Ci*) and the rank for each alternative were calculated using Equations (7)–(11), which are mentioned in Table 6. The results are ranked by the closeness coefficient values. A higher *Ci* indicates that the experimentally measured response is near to an optimal solution. The *Ci* values for individual experimental runs are shown in Figure 8. From the results of the TOPSIS approach, it is perceived that Experiment 1 has the highest Ci value of 0.53934; therefore, the corresponding processing parameters of FDM are considered as the best parameters for improved surface quality. Furthermore, the mean closeness coefficients for each parameter level are shown in Figure 9. From the figure, it is perceived that the optimal FDM parameters for improved surface quality characteristics are 0.228 mm layer thickness, 90° part orientation, 0.558 mm raster width and 0° raster angle. From Table 7, part orientation and raster width have maximum delta values among the selected parameters; therefore, these two parameters have a substantial influence on the surface quality characteristics of FDM-processed parts.

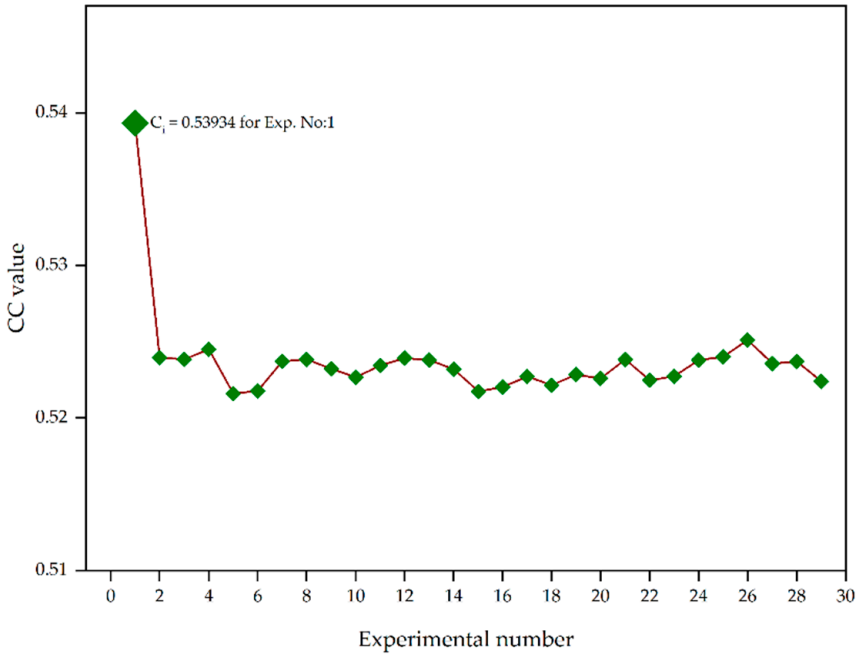

Figure 8. Closeness coefficient values for each experimental specimen.

Table 6. Weight normalized matrix, separation measures and rank.

Ex. No	Weight Normalized Values			*Si* PLUS	*Si* MINUS	*Ci*	Rank
	Ra	*Rz*	*Rq*				
1	**25.8**	**98.3**	**49.4**	**0.0185**	**0.0217**	**0.5393**	**1**
2	27.2	96.8	46.3	0.2221	0.2444	0.5240	5
3	25.9	95.9	47.0	0.2206	0.2428	0.5239	7
4	27.7	96.1	44.3	0.2187	0.2412	0.5245	3
5	23.4	104.1	48.6	0.2389	0.2605	0.5216	29
6	23.6	105.7	44.7	0.2385	0.2602	0.5218	27
7	27.5	98.1	46.4	0.2249	0.2473	0.5237	12
8	26.8	93.6	50.9	0.2205	0.2426	0.5238	9
9	26.6	96.3	51.2	0.2262	0.2483	0.5232	16
10	27.3	100.8	49.7	0.2339	0.2561	0.5227	21
11	26.7	98.5	46.8	0.2260	0.2482	0.5235	15
12	27.9	94.9	49.8	0.2221	0.2445	0.5239	6
13	27.1	97.3	46.6	0.2234	0.2457	0.5238	11
14	26.1	98.4	48.1	0.2270	0.2491	0.5232	17
15	22.2	102.1	48.8	0.2348	0.2562	0.5218	28
16	26.4	104.2	48.7	0.2397	0.2618	0.5220	26
17	26.5	101.3	47.8	0.2328	0.2549	0.5227	20
18	25.5	102.5	49.1	0.2364	0.2583	0.5222	25
19	26.9	99.4	49.9	0.2312	0.2533	0.5229	18
20	24.1	101.7	45.2	0.2306	0.2524	0.5226	22
21	27.5	97.5	46.5	0.2238	0.2462	0.5238	8
22	27.6	103.8	47.1	0.2375	0.2599	0.5225	23
23	24.5	99.8	47.5	0.2290	0.2508	0.5227	19
24	26.2	96.4	46.9	0.2216	0.2438	0.5238	10
25	27.4	96.5	46.7	0.2219	0.2443	0.5240	4
26	28.1	91.5	47.4	0.2126	0.2351	0.5251	2
27	27.8	100.4	44.2	0.2276	0.2501	0.5236	14
28	25.7	97.1	46.1	0.2221	0.2442	0.5237	13
29	27.0	102.9	48.3	0.2367	0.2589	0.5224	24

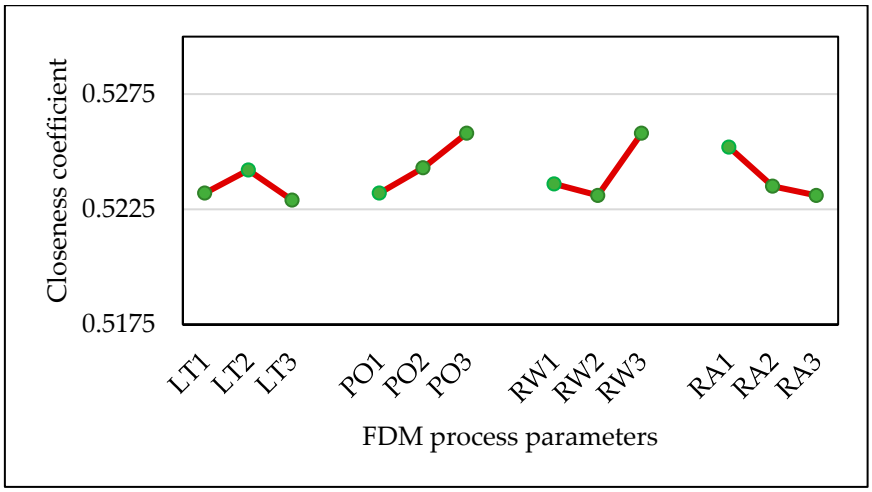

Figure 9. Mean closeness coefficients for FDM process parameters.

Table 7. Mean closeness coefficient for process parameters.

S. No	Process Parameters	Level 1	Level 2	Level 3	Delta	Rank
1	Layer thickness (A)	0.5232	0.5242	0.5229	0.0013	4
2	Part orientation (B)	0.5232	0.5243	**0.5258**	0.0026	2
3	Raster width (C)	0.5236	0.5231	**0.5258**	0.0027	1
4	Raster angle (D)	**0.5252**	0.5235	0.5231	0.0021	3

4.4. Design and Fabrication of Flapping Wing Micro Mechanism at Optimal FDM Conditions

The optimal FDM process parameters obtained through the TOPSIS approach were further utilized for fabricating the components of a flapping wing micro mechanism. The flapping wing micro components such as mechanism base, wing connector, long, medium, linkages and short bars for connecting the parts were designed and fabricated at a tolerance limit of 100 µm through the FDM process. The assembled flapping wing mechanism, shown in Figure 10, provided a smooth operation in extreme conditions without any slippage or wear of the contact surfaces. Furthermore, the surface profile of the fabricated flapping wing part was obtained through the 3D profilometer, as shown in Figure 11. From the profile, a smooth surface with an average *Ra* of 20.6 µm was achieved for the assembly of a flapping wing micro mechanism through optimized FDM parameters.

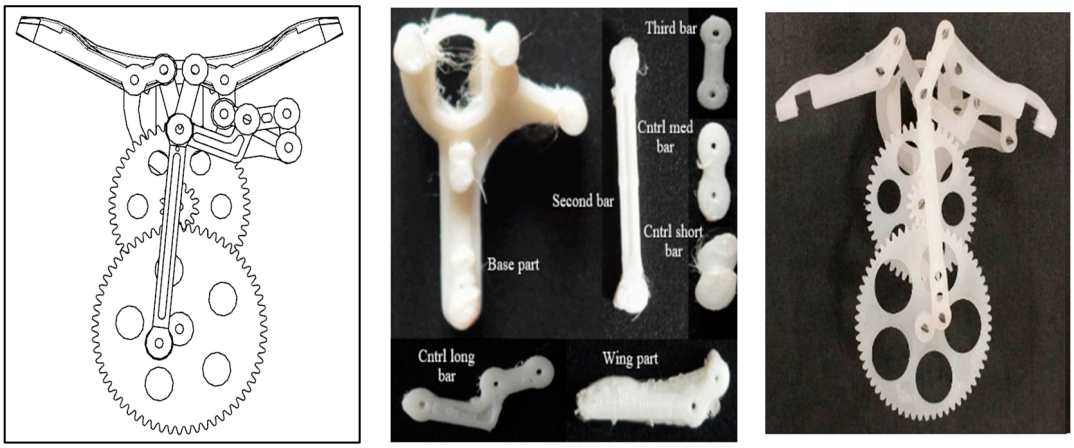

Figure 10. Design and fabricated flapping wing micro mechanism assembly with optimal FDM processing conditions.

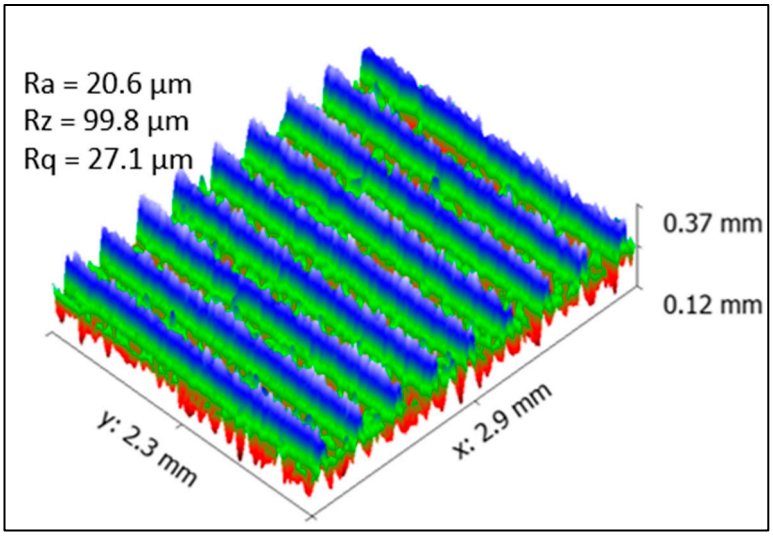

Figure 11. Three-dimensional surface profile of flapping wing mechanism part fabricated with optimal FDM parameter settings.

5. Conclusions

The present work investigated the surface roughness characteristics of FDM-fabricated ABS specimens under different processing conditions, and optimization was carried out to identify the optimal process parameters for the improved surface quality of micro mechanical components. The following conclusions can be drawn from the performed experimental, statistical and optimization studies.

- The ANOVA results showed that the selected FDM parameters have a substantial influence on surface roughness properties. The part orientation and raster angle have the most significant influence on *Ra*. Layer thickness and raster width are the most influential parameters on *Rz*, whereas *Rq* is primarily influenced by layer thickness and raster angle.
- The optimal FDM parameters were attained through the TOPSIS optimization approach, namely layer thickness of 0.2285 mm, part orientation of 45°, raster width of 0.558 mm and raster angle of 0°, for the improved surface quality features of *Ra* = 25.8 µm, *Rz* = 98.3 µm and *Rq* = 49.4 µm.
- The surface micrographs of FDM-fabricated parts with different processing parameters were investigated through SEM analysis, and we found abbreviated surface cracks, voids and overlapping layers at a higher layer thickness.
- Finally, the components of a flapping wing micro mechanism were fabricated under optimal FDM conditions and assembled to investigate their performance. The improved surface quality of the flapping wing components provided smooth and defect-free operations; thus, the life cycle of dynamic components can be improved significantly.
- The current study looked into the most influential FDM parameters on the surface quality of produced ABS parts. Future research could focus on the dynamic and thermomechanical properties of micro mechanical components manufactured using the FDM technique.

Author Contributions: Conceptualization, D.R. and E.B.; Methodology, D.R., L.-J.Y. and E.B.; Experimental Design, D.R.; Experimental Setup, D.R., L.-J.Y. and E.B.; Experiments, D.R. and E.B.; Measurements, D.R., L.-J.Y. and E.B.; Investigation, D.R., E.B. and L.-J.Y.; Resources, D.R., E.B. and L.-J.Y.; Visualization, D.R., E.B. and L.-J.Y.; Writing—Original Draft Preparation, D.R., E.B. and L.-J.Y.; Writing—Review and Editing, D.R., E.B. and L.-J.Y.; Supervision, E.B. and L.-J.Y.; Project Administration, D.R. and E.B.; Funding Acquisition, D.R., E.B. and L.-J.Y. All authors have read and agreed to the published version of the manuscript.

Funding: This research was funded by the Ministry of Science and Technology, Taiwan (grant numbers 109-2221-E-032-002-MY2, 109-2221-E-032-001-MY3 and 111-2923-E-032-001-MY3).

Conflicts of Interest: The authors declare no conflict of interest.

References

1. Yang, L.-J.; Esakki, B.; Chandrasekhar, U.; Hung, K.-C.; Cheng, C.-M. Practical Flapping Mechanisms for 20 cm-span Micro Air Vehicles. *Int. J. Micro Air Veh.* **2015**, *7*, 181–202. [CrossRef]
2. Esakki, B.; Mathiyazhagan, S.; Moses, M.; Rao, K.J.; Ganesan, S. Development of 3D-printed floating Quadrotor for collection of algae in remote water bodies. *Comput. Electron. Agric.* **2019**, *164*, 104891. [CrossRef]
3. Udayagiri, C.; Kulkarni, M.; Esakki, B.; Pakiriswamy, S.; Yang, L.J. Experimental Studies on 3D Printed Parts for Rapid Prototyping of Micro Aerial Vehicles. *J. Appl. Sci. Eng.* **2016**, *19*, 17–22.
4. Rajamani, D.; Balasubramanian, E.; Arunkumar, P.; Silambarasan, M.; Bhuvaneshwaran, G. Experimental Investigations and Parametric Optimization of Process Parameters on Shrinkage Characteristics of Selective Inhibition Sintered High Density Polyethylene Parts. *Exp. Tech.* **2018**, *42*, 631–644. [CrossRef]
5. Esakki, B.; Rajamani, D.; Arunkumar, P. Modeling and prediction of optimal process parameters in wear behaviour of selective inhibition sintered high density polyethylene parts. *Prog. Addit. Manuf.* **2018**, *3*, 109–121. [CrossRef]
6. Altan, M.; Eryıldız, M.; Gumus, B.; Kahraman, Y. Effects of process parameters on the quality of PLA products fabricated by fused deposition modeling (FDM): Surface roughness and tensile strength. *Mater. Test.* **2018**, *60*, 471–477. [CrossRef]
7. Campbell, R.; Martorelli, M.; Lee, H. Surface roughness visualisation for rapid prototyping models. *Comput. Des.* **2002**, *34*, 717–725. [CrossRef]
8. Yang, L.; Li, S.; Li, Y.; Yang, M.; Yuan, Q. Experimental Investigations for Optimizing the Extrusion Parameters on FDM PLA Printed Parts. *J. Mater. Eng. Perform.* **2019**, *28*, 169–182. [CrossRef]
9. Yash, M.; Divyansh, P.; Akash, B.; Shantanu, H.; Vasudev, P.; Mahesh, S.K. Process Parameter Optimization for FDM 3D Printer. *Int. Res. J. Eng. Technol.* **2019**, *6*, 1–6.
10. Boddula, V.; Manzoor, H.; Chintireddy, S.R. Optimization of 3D Printing Process Parameters of Poly Lactic Acid Materials by Fused Deposition Modeling Process. *Int. J. Eng. Develop. Res.* **2019**, *7*, 189–196.

11. Camargo, J.C.; Machado, R.; Almeida, E.C.; Silva, E.F.M.S. Mechanical properties of PLA-graphene filament for FDM 3D printing. *Int. J. Adv. Manuf. Technol.* **2019**, *103*, 2423–2443. [CrossRef]
12. Vigneshwaran, K.; Venkateshwaran, N. Statistical analysis of mechanical properties of wood-PLA composites prepared via additive manufacturing. *Int. J. Polym. Anal. Charact.* **2019**, *24*, 584–596. [CrossRef]
13. Ferro, C.; Grassi, R.; Seclì, C.; Maggiore, P. Additive Manufacturing Offers New Opportunities in UAV Research. *Procedia CIRP* **2016**, *41*, 1004–1010. [CrossRef]
14. Hsu, C.-K.; Evans, J.; Vytla, S.; Huang, P.G. Development of flapping wing micro air vehicles—Design, CFD, experiment and actual flight. In *48th AIAA Aerospace Sciences Meeting Including the New Horizons Forum and Aerospace Exposition*; American Institute of Aeronautics and Astronautics: Reston, VA, USA, 2010.
15. Richter, C.; Lipson, H. Untethered Hovering Flapping Flight of a 3D-Printed Mechanical Insect. *Artif. Life* **2011**, *17*, 73–86. [CrossRef] [PubMed]
16. Yen, H.-J.; Tseng, C.-S.; Hsu, S.-H.; Tsai, C.-L. Evaluation of chondrocyte growth in the highly porous scaffolds made by fused deposition manufacturing (FDM) filled with type II collagen. *Biomed. Microdevices* **2009**, *11*, 615–624. [CrossRef]
17. Kalita, S.J.; Bose, S.; Hosick, H.L.; Bandyopadhyay, A. Development of controlled porosity polymer-ceramic composite scaffolds via fused deposition modeling. *Mater. Sci. Eng. C* **2003**, *23*, 611–620. [CrossRef]
18. Zein, I.; Hutmacher, D.W.; Tan, K.C.; Teoh, S.H. Fused deposition modeling of novel scaffold architectures for tissue engineering applications. *Biomaterials* **2002**, *23*, 1169–1185. [CrossRef]
19. Tirella, A.; de Maria, C.; Criscenti, G.; Vozzi, G.; Ahluwalia, A. The PAM2system: A multilevel approach for fabrication of complex three-dimensional microstructures. *Rapid Prototyp. J.* **2012**, *18*, 299–307. [CrossRef]
20. Devaraj, R.; Mahalingam, S.K.; Esakki, B.; Astarita, A.; Mirjalili, S. A hybrid GA-ANFIS and F-Race tuned harmony search algorithm for Multi-Response optimization of Non-Traditional Machining process. *Expert Syst. Appl.* **2022**, *199*, 116965. [CrossRef]
21. Ananthakumar, K.; Rajamani, D.; Balasubramanian, E.; Davim, J.P. Measurement and optimization of multi-response characteristics in plasma arc cutting of Monel 400™ using RSM and TOPSIS. *Measurement* **2018**, *135*, 725–737. [CrossRef]
22. Galantucci, L.; Lavecchia, F.; Percoco, G. Experimental study aiming to enhance the surface finish of fused deposition modeled parts. *CIRP Ann.* **2009**, *58*, 189–192. [CrossRef]
23. Sachdeva, A.; Singh, S.; Sharma, V.S. Investigating surface roughness of parts produced by SLS process. *Int. J. Adv. Manuf. Technol.* **2013**, *64*, 1505–1516. [CrossRef]
24. Sood, A.K.; Ohdar, R.K.; Mahapatra, S.S. Parametric appraisal of fused deposition modelling process using the grey Taguchi method. *Proc. Inst. Mech. Eng. Part B J. Eng. Manuf.* **2010**, *224*, 135–145. [CrossRef]
25. Pérez, M.; Medina-Sánchez, G.; García-Collado, A.; Gupta, M.; Carou, D. Surface Quality Enhancement of Fused Deposition Modeling (FDM) Printed Samples Based on the Selection of Critical Printing Parameters. *Materials* **2018**, *11*, 1382. [CrossRef] [PubMed]
26. Sood, A.K.; Chaturvedi, V.; Datta, S.; Mahapatra, S.S. Optimization of process parameters in fused deposition modeling using weighted principal component analysis. *J. Adv. Manuf. Syst.* **2011**, *10*, 241–259. [CrossRef]
27. Sood, A.K.; Ohdar, R.; Mahapatra, S. Improving dimensional accuracy of Fused Deposition Modelling processed part using grey Taguchi method. *Mater. Des.* **2009**, *30*, 4243–4252. [CrossRef]
28. Byun, H.-S.; Lee, K.H. Determination of the optimal build direction for different rapid prototyping processes using multi-criterion decision making. *Robot. Comput. Manuf.* **2006**, *22*, 69–80. [CrossRef]
29. Durgun, I.; Ertan, R. Experimental investigation of FDM process for improvement of mechanical properties and production cost. *Rapid Prototyp. J.* **2014**, *20*, 228–235. [CrossRef]
30. Fatimatuzahraa, A.; Farahaina, B.; Yusoff, W. The effect of employing different raster orientations on the mechanical properties and microstructure of Fused Deposition Modeling parts. In Proceedings of the 2011 IEEE Symposium on Business, Engineering and Industrial Applications (ISBEIA), Langkawi, Malaysia, 25–28 September 2011; IEEE: Amsterdam, The Netherlands, 2011. [CrossRef]
31. Mohanraj, R.; Elangovan, S.M.; Arunkarthik, B.; Pratheesh Kumar, S.K.; Maaz Baig, N.B.; Shriram, A.; Muneeskumar, M. Effect of process parameters on tensile strength and surface quality of PLA-ABS part produced by fused deposition modeling. *Ind. J. Eng. Mater. Sci.* **2021**, *28*, 300–310.